A STATIONARY CYLINDRICAL WIND SPEED AND DIRECTION SENSOR FOR USE IN MODEL TESTING

James L. Amick
Department of Aerospace Engineering

Gerald C. Gill
Department of Meteorology and Oceanography

Presented at the

International Research Seminar:
Wind Effects on Buildings and Structures
11-15 September, 1967
Ottawa, Canada

The University of Michigan
Ann Arbor, Michigan

September, 1967

TABLE OF CONTENTS

LIST OF FIGURES

SUMMARY

A miniature wind speed and direction sensor has been developed for use on wind tunnel models of towers or structures. The sensor was developed to permit simulation of 1/100 scale models (or larger) of standard wind speed and direction sensors on standard meteorological towers, but it can be used for other model testing.

The sensor consists of a vertical cylinder 0.25 inch in diameter by 0.62 inch in length with nine radial holes 40° apart about the mid-diameter. Each hole is connected by capillary tubing to its own manometer. Support of the sensor is by a sheath covering the nine stainless steel capillary tubes. The spacing of the orifices is accurate within ± 1/4 degree. The orifices are connected to a bank of nine inclined manometers that measure the pressure difference between each orifice and the static pressure in the tunnel. Measurements are made during steady flow conditions in the tunnel.

One sensor was calibrated in a University of Michigan wind tunnel through a Reynolds number range of 16,000 to 128,000, and for wind speeds below 150 mph (Mach number 0.2). It measured wind speed to within 1.3% and wind direction to within 0.6°. When the wind striking the sensor deviated from the horizontal by ± 15° , the indicated speed was up to 3% too low and the indicated direction was in error by up to ± 1.2°.

INTRODUCTION

A circular cylinder with vertical axis can be used to measure the horizontal components of wind velocity. Such a cylindrical wind-velocity sensor has many of the advantages of a propeller-type anemometer-wind vane. In addition, it has no moving parts and can, therefore, be made much smaller than a propeller-type anemometer-wind vane.

The cylindrical wind-velocity sensor makes use of the nearly sinusoidal pressure distribution over most of the windward side of a circular cylinder. Three pressure measurements in the sinusoidal-pressure region are enough to determine the amplitude and phase of the sine curve, and from these the wind speed and direction may be calculated.

In order to calibrate a cylindrical wind-velocity sensor, the pressure distribution over the windward side of the cylinder must be obtained at known wind velocities. Although such data are available for infinite cylinders (see, for example, Reference 1), the special case of a short cylinder mounted on a rather large support shaft does not seem to have been previously treated.

The present tests were made on a cylinder 2.5 diameters long and mounted at one end on a coaxial support shaft whose diameter was .75 or .88 of the cylinder diameter. Reynolds number based on cylinder diameter ranged from 16,000 to 128,000 and the Mach number was .21 or less.

The sensor was developed for wind tunnel testing of tower models as small as 1/100 full scale.

APPARATUS AND TESTS

The tests were conducted in the five- by seven-foot low turbulence wind tunnel of the University of Michigan. The models were mounted on the tunnel balance system, and the motorized yaw drive of the balance was used to provide rotation about the vertical axis (cylinder axis). The angular position of the models was measured on a twelve-inch-diameter protractor graduated in one-half-degree intervals. Provision was also made for rotation about a horizontal axis, so that the angle between the cylinder axis and the wind direction (normally 90°) could be varied.

Two models were tested: a one-inch-diameter model and a one-fourth-inch-diameter model. A sketch of the latter is shown in Figure 1 and a photograph in Figure 2. The one-inch-diameter model was geometrically similar except that its orifices lacked the 60°-tapered enlargement (a manufacturing expediency), and coarse sandpaper replaced the knurled areas. (Preliminary tests showed that without sandpaper or knurling, laminar separation occurred within 60° of the stagnation point; adding roughness to much of the cylinder area moved the separation point beyond 70°). For most of the tests the cavity at the top of the model was filled with clay.

Both models were inspected by means of a microscope, and in each case it was found that the spacing of orifices was accurate to within $\pm \frac{1}{4}$ degree. The alignment holes were also properly oriented to within $\pm \frac{1}{4}$ degree.

The initial alignment of each model in the tunnel was made by means of a telescope. The telescope was positioned so that a line through

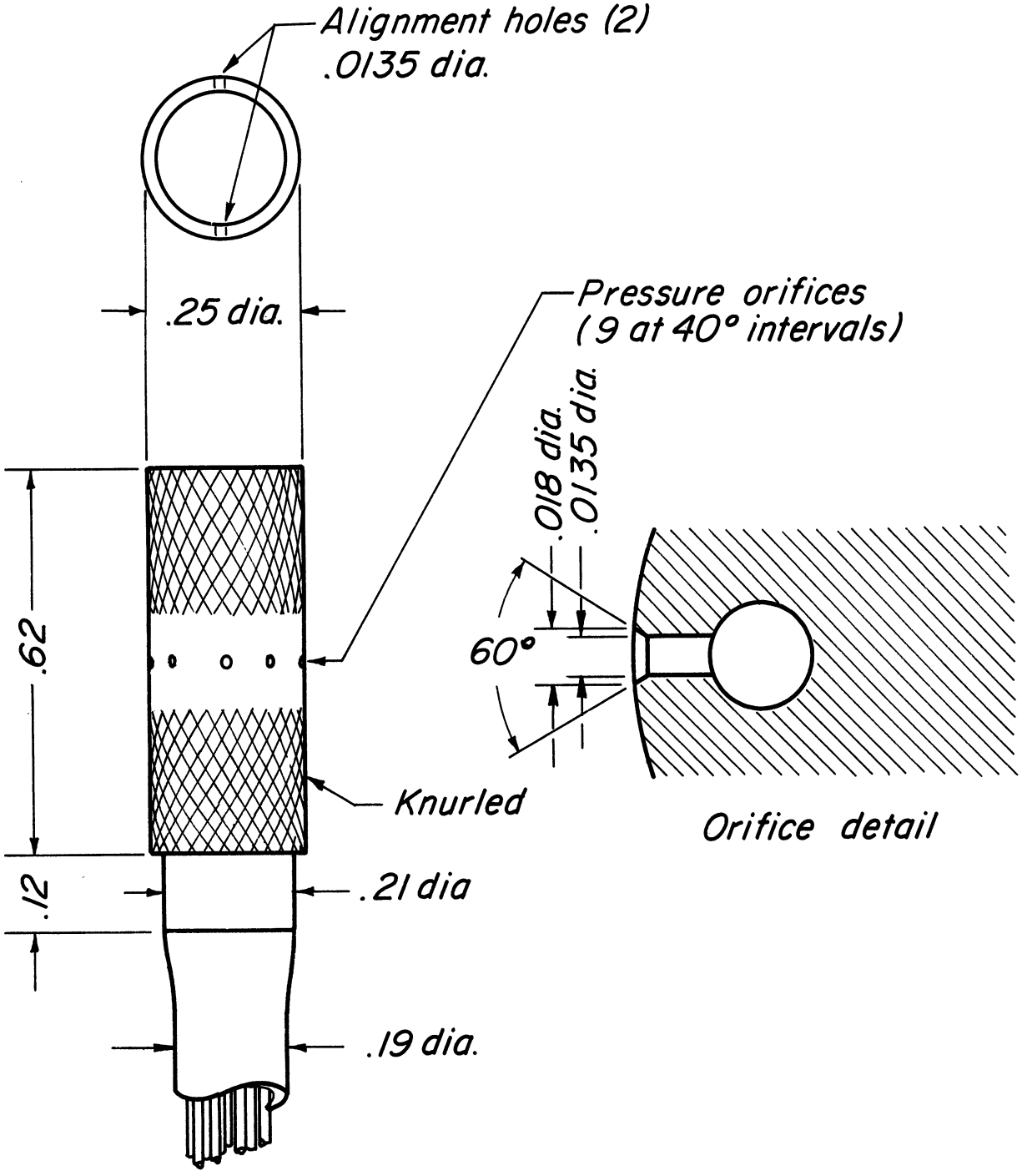

Figure 1. Cylindrical Wind-Velocity Sensor, (One-fourth-inch model).

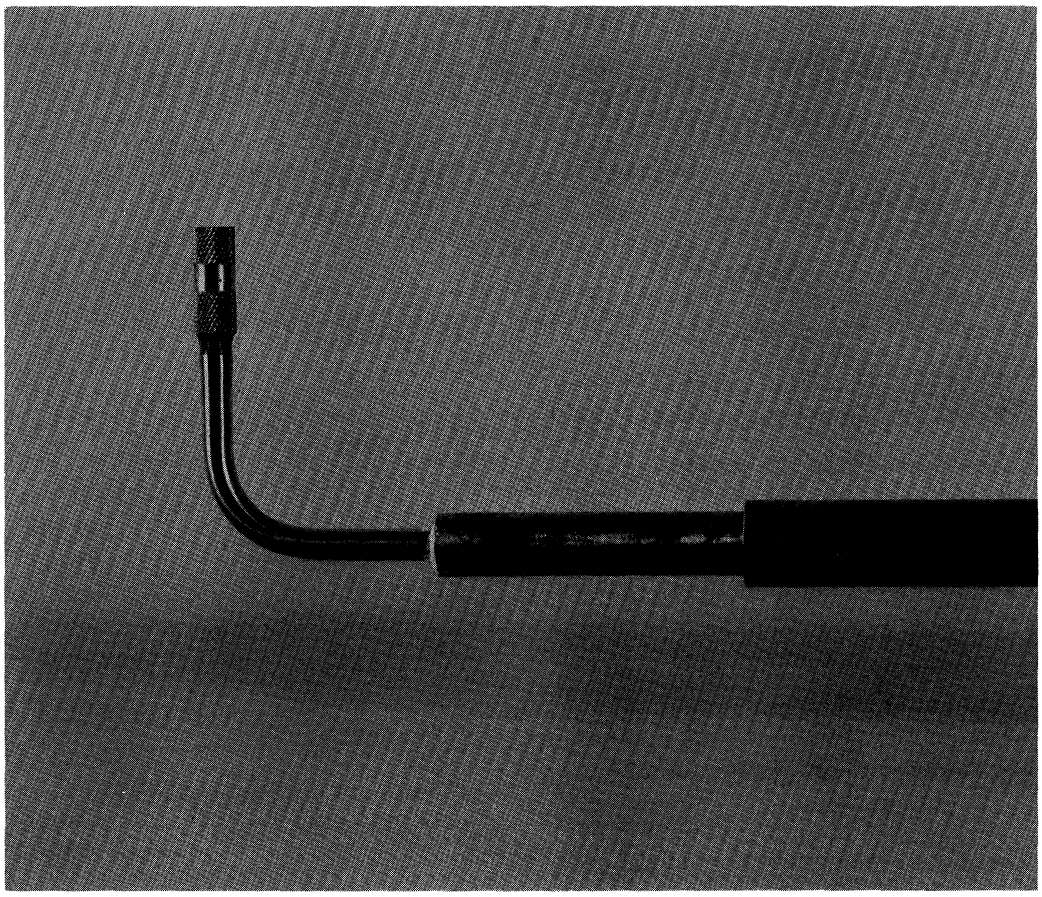

Figure 2. Photograph of Wind-Velocity Sensor, (One-fourth-inch model).

its axis and the axis of the model was parallel to the tunnel center-line. The model was then rotated until the image of the two alignment holes was as nearly circular as possible. The zero position obtained in this manner was found to be repeatable within $\pm \frac{1}{4}$ degree.

Pressures on the models were measured by means of an inclined multiple-tube manometer board using water as the indicating fluid. The tunnel static and stagnation pressures were also indicated on the same manometer board. The inclination of the manometer was adjusted so that the difference between the static and stagnation readings was a convenient number of inches, say five inches, and the liquid level was adjusted so that both readings were in exact whole inches. The manometer scale was then re-labeled so that the model pressures could be easily read as values of $\Delta p/q$, with each inch representing, in this case, $.2q$. At the higher speeds this procedure was modified to take account of compressibility effects.

RESULTS AND DISCUSSION

The main results of the tests are shown in Figure 3 as the circumferential variation of pressure coefficient, corrected for compressibility effects, for three different Reynolds numbers. (The compressibility correction is based on the data of Reference 2, which show that in the region within 60° of the stagnation point, the compressibility effect Mach numbers of .4 or less can be well approximated as an increment of $M^2/4$ to the pressure coefficients). The measured data are shown along with empirical curves based on the relation

$$\frac{\Delta p}{q} - \frac{M^2}{4} = 1 - \frac{2.925}{\left(1 + \frac{21.85}{\sqrt{Re}}\right)} \sin^2 1.047\,\phi \qquad (1)$$

where the pressure coefficient is defined as

$$\frac{\Delta p}{q} = \frac{p - p_s}{\frac{1}{2}\rho S^2}$$

the Reynolds number is defined as

$$Re = \frac{S d \rho}{\mu}$$

p is the local pressure, p_s is the free stream static pressure, ρ is the mass density of the fluid, S is the free stream velocity, d is the diameter of the cylinder, μ is the viscosity of the fluid, M is the free stream Mach number, and ϕ is the angular distance around the circumference of the cylinder, measured from the stagnation point.

Most of the data points of Figure 3 represent the averages of two nearly equal measurements. Almost all of the measurements were made with the top of the sensor filled with clay; however, data from the tests

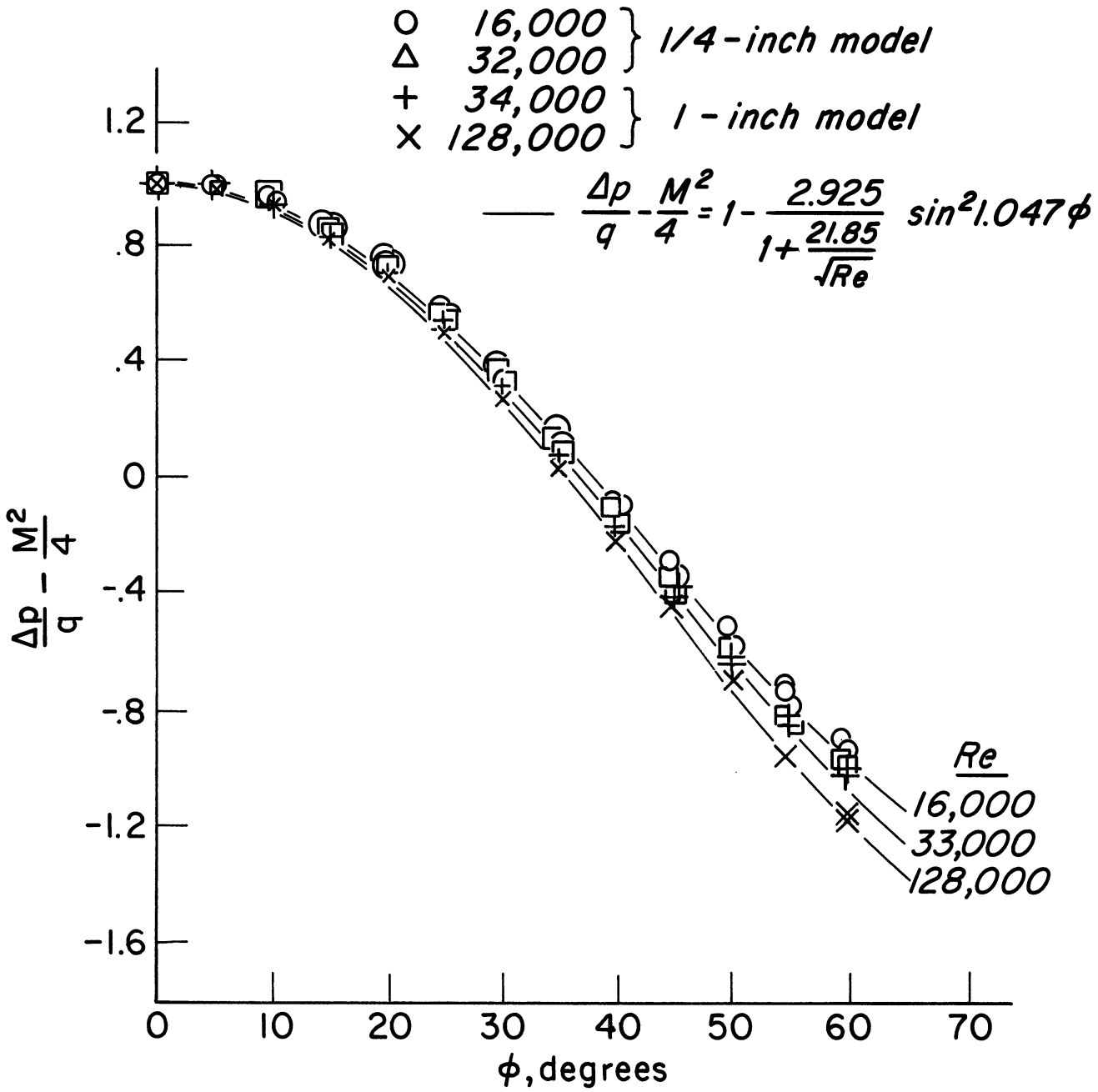

Figure 3. Pressure Coefficient Distribution Around Forward Part of Cylindrical Wind-Velocity Sensor.

that were made with the top open are included in the figure and fall within the scatter of the other data.

The test data show a tendency toward higher pressures than those given by the sine curves, especially in the regions $5° < \phi < 30°$ and $\phi > 50°$. The high pressures in the first of these regions may be due to the relatively large orifice size compared to the cylinder diameter. A similar orifice-size effect was noted in Reference 3. The departure from the sine curves beyond 50° may be due to proximity to separation, which occurred in the neighborhood of 70°.

Equation (1) gives a relationship between the pressures measured on the forward part of the cylinder and the speed of the stream in which it is immersed. Using Equation (1) the speed of an unknown stream can be written in terms of the pressures measured at three orifices spaced 40° apart as (see the appendix)

$$S = \sqrt{\frac{1.03 + \frac{22.6}{\sqrt{Re}}}{\rho}} \sqrt{(\Delta p_A)^2 - .22\, \Delta p_A\, \Delta p_B + (\Delta p_B)^2} \qquad (2)$$

where

$$\Delta p_A = p_m - p_{(m-1)}$$
$$\Delta p_B = p_{(m+1)} - p_m$$

and the subscripts indicate the orifice number, going clockwise as viewed from above the sensor, with the orifice having the highest pressure designated as the m-th orifice. This equation can be easily solved by making a first approximation to the Reynolds number, calculating S, and using this S to determine a second approximation to the Reynolds

number with which a second approximation to S may be calculated. Because of the weak influence of Re in Equation (2), the second approximation should be quite accurate.

The empirical relation of Equation (1) was chosen to minimize the scatter in speeds calculated by means of Equation (2) from the data shown in Figure 3. As shown in Figure 4, the largest error in calculated speed for any of the data of Figure 3 is 1.3%. At the highest Reynolds number tested the largest error is only .6%.

The periodic nature of the errors shown in Figure 4 is due to the systematic deviation of the pressure distribution from a sine curve, as pointed out in connection with Figure 3. These errors could, therefore, be reduced by using smaller orifices, which would reduce the orifice-size effect. However, this would increase the response time of the pressure measuring system, so that a longer time would be required to reach pressure equilibrium.

The effect of a flow velocity component in the direction of the cylinder axis, on the error in calculated speed is shown in Figure 5. For upflow speeds less than .15 of the normal speed, the error due to the upflow appears to be less than 2%, but may reach 6% for an upflow velocity ratio of .26 (upflow angle, Θ, of 15°).

The flow direction can also be determined from the pressure differences at the three forward orifices through the equation (derived in the appendix)

$$\phi = 40(m-1) + .478 \sin^{-1}\left[\frac{.667(\Delta p_A + \Delta p_B)}{\sqrt{(\Delta p_A)^2 - .22\,\Delta p_A\,\Delta p_B + (\Delta p_B)^2}}\right] \quad (3)$$

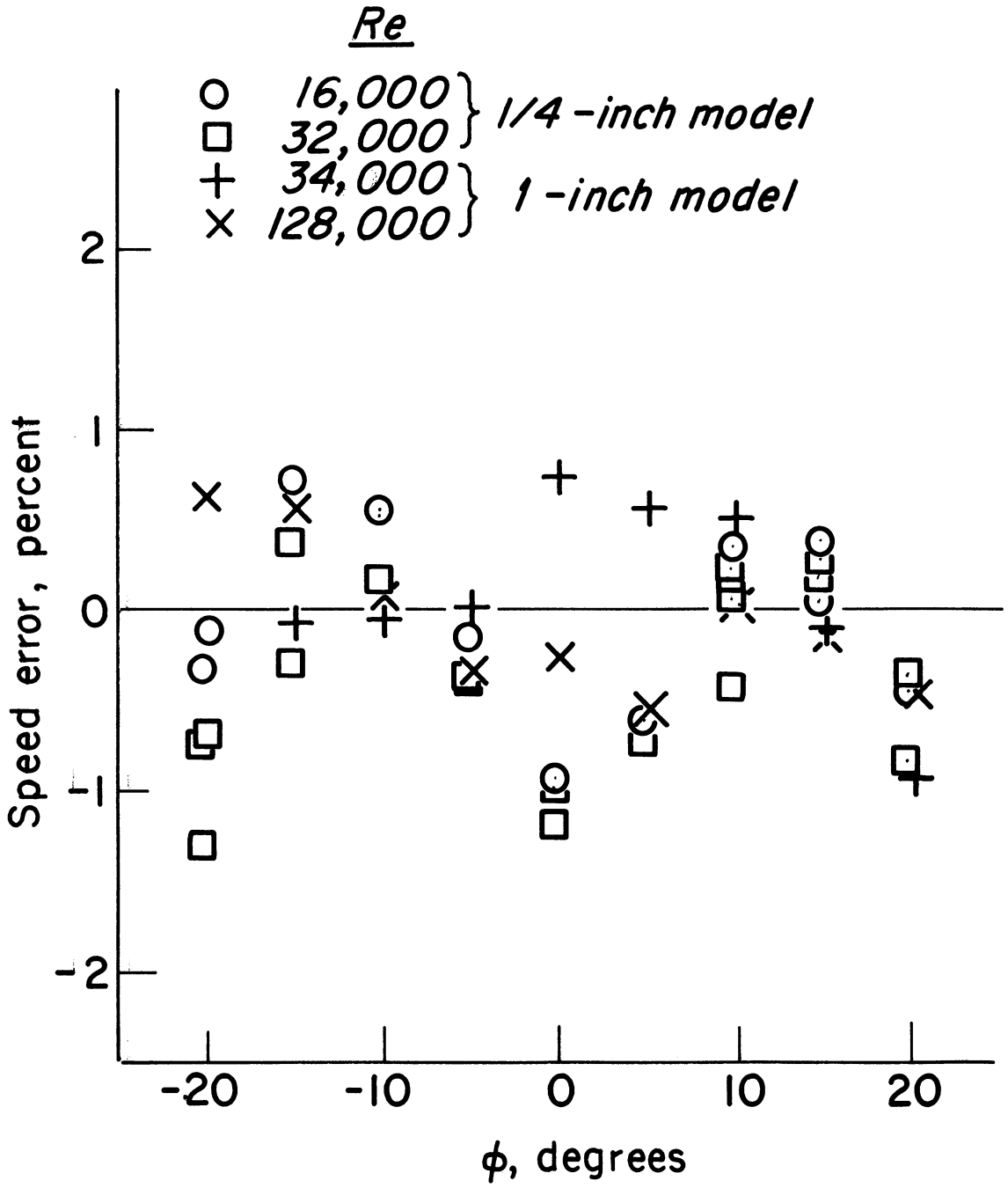

Figure 4. Error in Indicated Speed as a Function of Angular Position of Highest-Pressure Orifice.

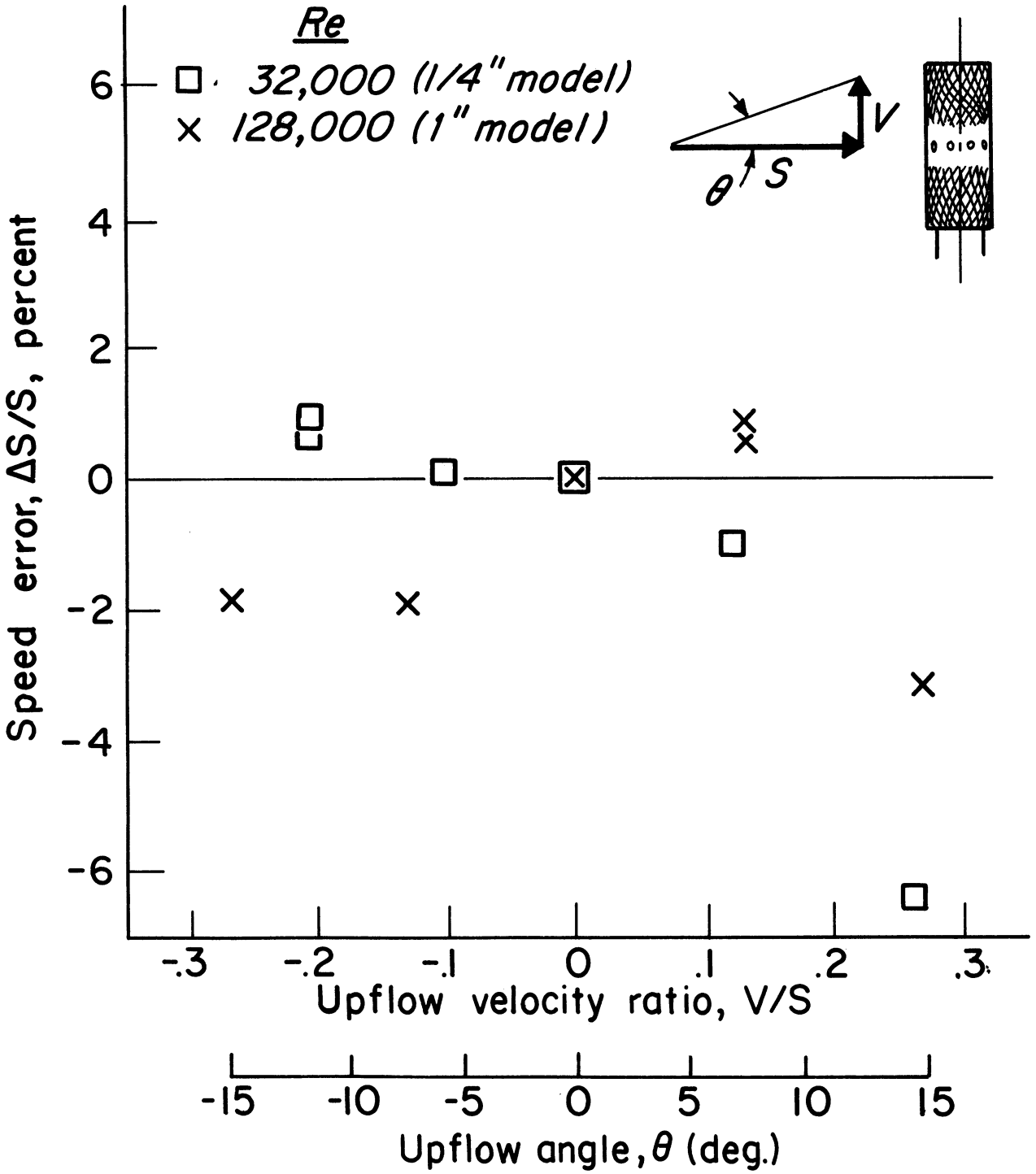

Figure 5. Error in Indicated Speed as a Function of Upflow Velocity.

The errors in flow angle calculated from the data of the calibration runs are shown in Figure 6. Most of the data shown are for zero upflow, but the points plotted at -4° and at .7° are for the upflow velocity ratios shown in Figure 5.

For this sensor, for zero upflow, the maximum flow-direction error is less than .6 degree. For finite upflow, the maximum error may become as large as 1.2 degree (obtained from the data for Re = 32,000 by adding the largest increment in flow angle error above the zero-upflow data (about .8°) to the largest positive flow angle error without upflow (about .4°).

Ten of these $\frac{1}{4}$-inch diameter wind velocity sensors were fabricated for the National Aeronautics and Space Administration under a subcontract with Ammann and Whitney, Incorporated.* These were installed at the Aerovane locations on a 1/8 scale, two-dimensional model of the Kennedy Space Center Meteorological Tower and on a 3% scale model of the Launch Complex 39 Mobile Support Structure as used at Cape Kennedy. The testing of these models with these new probes was done at NASA's Langley Research Center, Hampton, Virginia in the sixteen- by sixteen-foot Langley Transonic Dynamics Wind Tunnel. A section of the scaled-down meteorological tower with three probes on it is shown in Figure 7, and a close-up of one of the probes on the tower model is shown in Figure 8. The wind tunnel study is nearing completion at time of writing.

---

* Ammann and Whitney, Incorporated, 111 Eighth Avenue, New York, N.Y., -Consulting engineers.

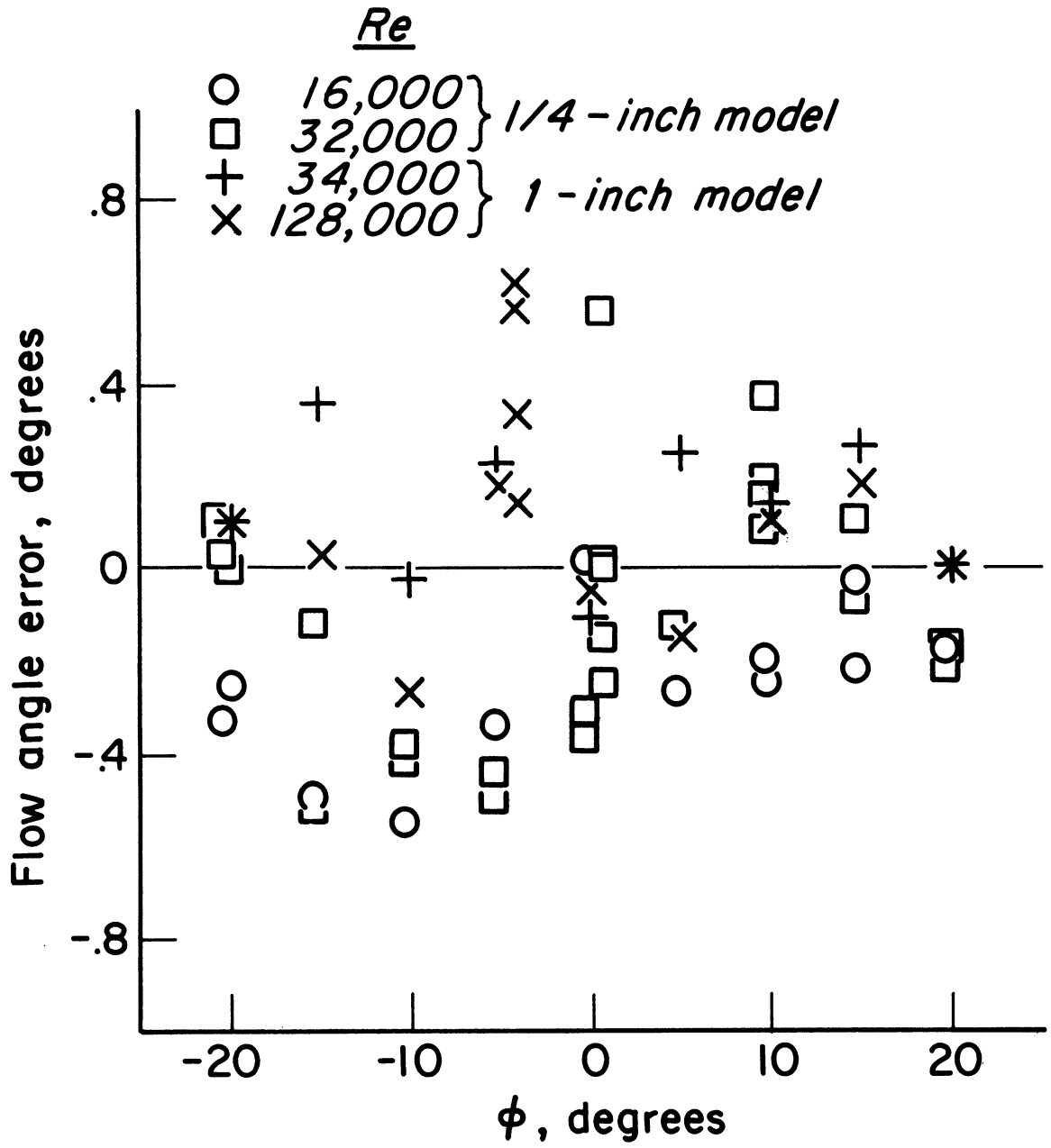

Figure 6. Error in Indicated Flow Direction as a Function of Angular Position of Highest-Pressure Orifice.

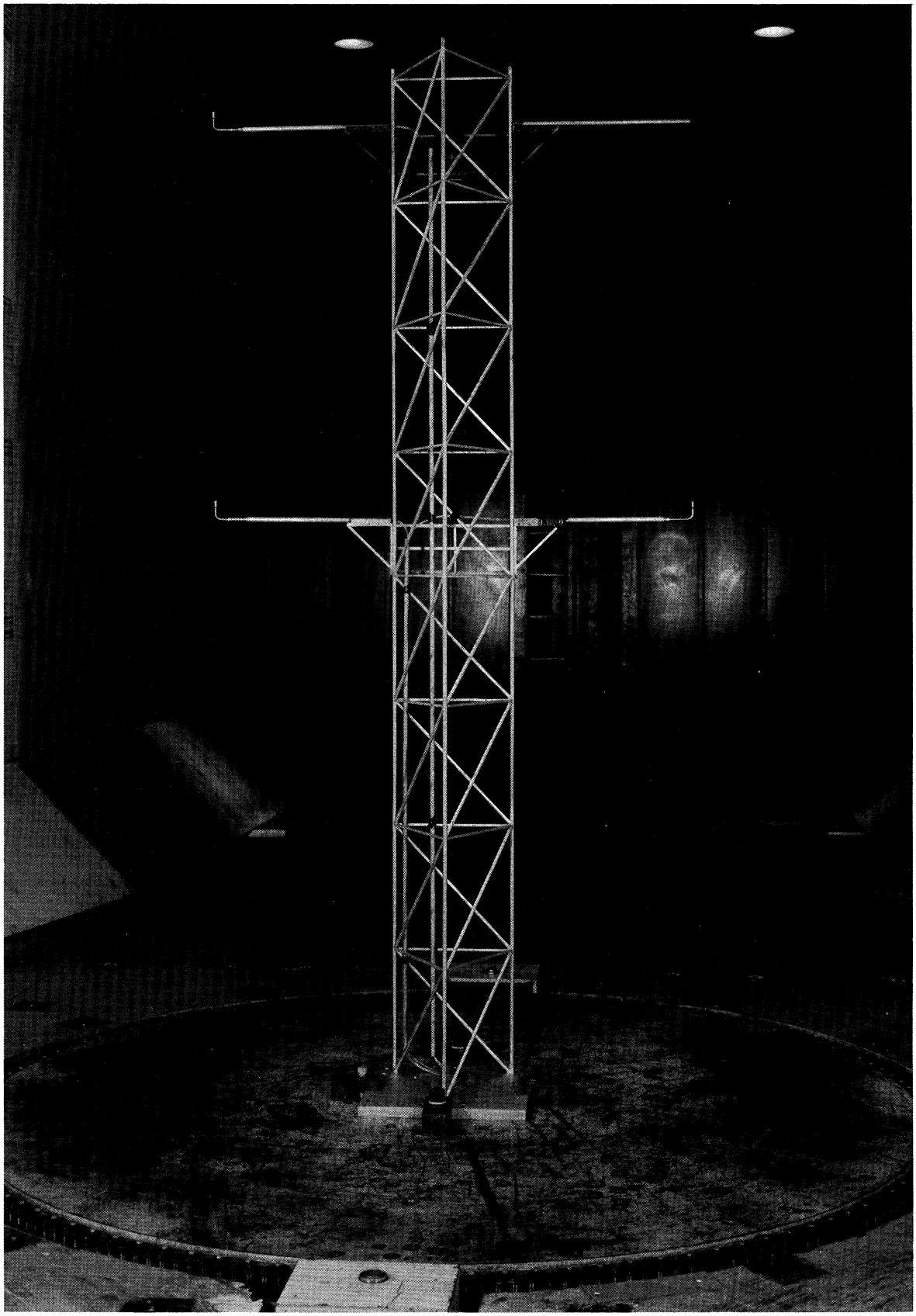

Figure 7. Section of 1/8-scale Model of Kennedy Space Center Meteorological Tower with Three Probes in Place. Tower section is in test position in sixteen- by sixteen-foot Langley Transonic Dynamics Wind Tunnel.

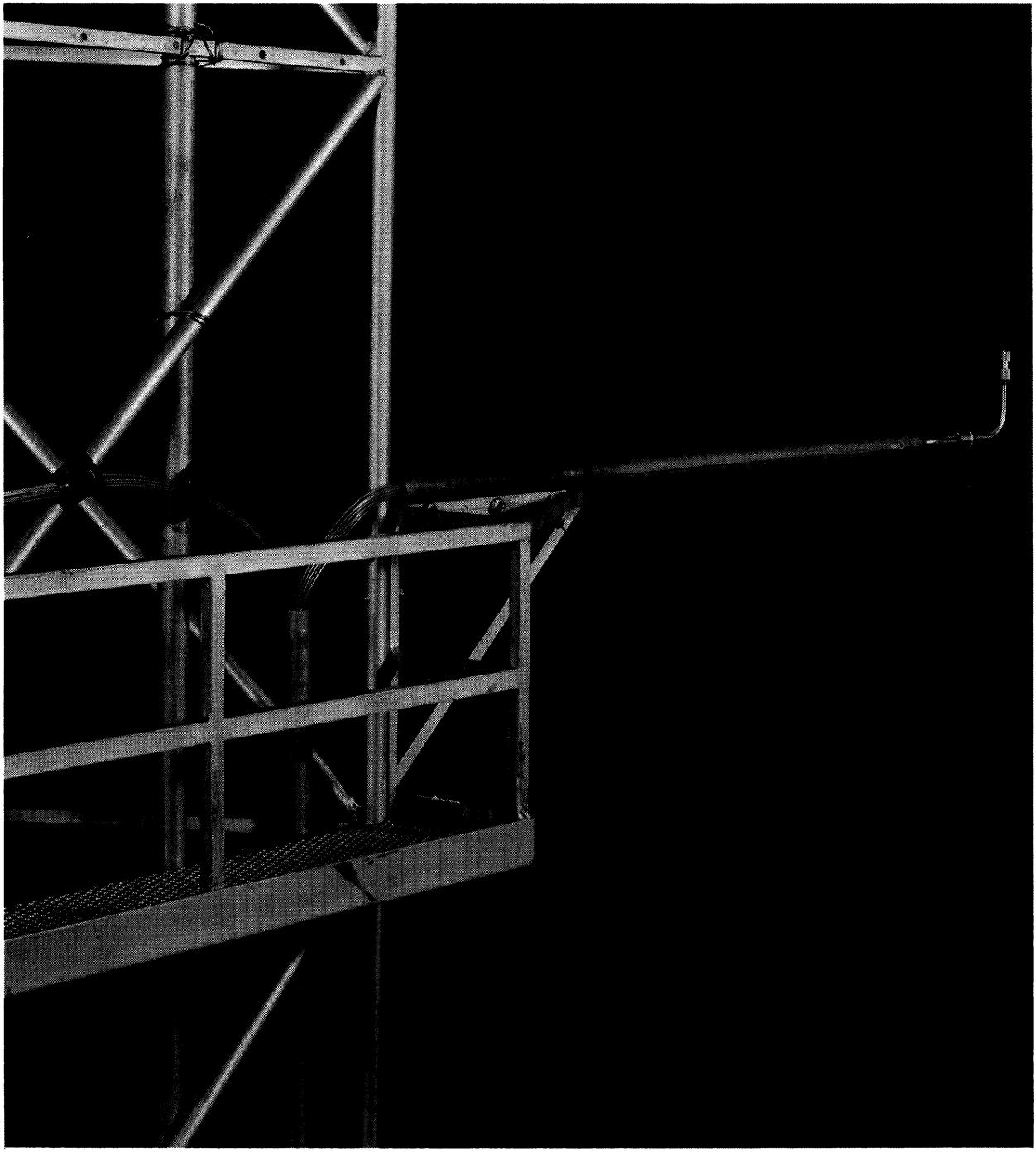

Figure 8. Close-up of Probe and Capillary Tube Mounting on Tower Model.

CONCLUSIONS

Over the Reynolds number range 16,000-128,000, the cylindrical wind-velocity sensor measures wind speed to within $\pm$ 1.3 percent and wind direction to within $\pm$ 0.6 degree. In the presence of a vertical wind component, the sensor (with axis vertical) measures the horizontal wind speed component with an error of less than $\pm$ 1.5 percent for upflow velocity ratios less than $\pm$ .1 but an error of up to 6.3% (too low) for upflow velocity ratios of 0.26 (upflow angle of 15°). The maximum wind direction error increases from 0.6 degree for zero upflow to 1.2 degrees for an upflow velocity ratio of .26.

ACKNOWLEDGMENTS

The writers are indebted to NASA and to Ammann and Whitney, Incorporated for the funds to support the development and testing of this new wind sensor. They are indebted to Mr. Robert Desmarais, Langley Research Center, for supplying the photographs of Figures 2, 7, and 8.

APPENDIX

The pressure distribution over the forward part of a circular cylinder can be approximated by

$$\frac{p-p_s}{q} = 1 + \frac{M^2}{4} - A \sin^2 (B \phi) \qquad (A1)$$

Rewrite this as

$$p = p_s + a\, q + b\, q \cos(c \phi) \qquad (A2)$$

where

$$a = \frac{M^2}{4} - \frac{A}{2} + 1$$

$$b = A/2$$

$$c = 2 B$$

Then the pressures at three consecutive orifices are

$$p_1 = p_s + a\, q + b\, q \cos(c \phi_1) \qquad (A3)$$

$$p_2 = p_s + a\, q + b\, q \cos(c \phi_2) \qquad (A4)$$

$$p_3 = p_s + a\, q + b\, q \cos(c \phi_3) \qquad (A5)$$

For nine equi-spaced orifices

$$\phi_1 = \phi_2 - \frac{2\pi}{9}$$

$$c\, \phi_1 = c\, \phi_2 - \frac{2\pi c}{9}$$

$$\cos(c \phi_1) = \cos(c \phi_2) \cos(2\pi c/9) + \sin(c \phi_2) \sin(2\pi c/9) \qquad (A6)$$

Similarly

$$\cos(c\,\phi_3) = \cos(c\,\phi_2)\cos(2\pi c/9) - \sin(c\,\phi_2)\sin(2\pi c/9) \quad (A7)$$

Equations (A3) and (A5) become, through (A6) and (A7),

$$p_1 = p_s + a\,q + b\,q\cos(c\,\phi_2)\cos(2\pi c/9) + b\,q\sin(c\,\phi_2)\sin(2\pi c/9) \quad (A8)$$

$$p_3 = p_s + a\,q + b\,q\cos(c\,\phi_2)\cos(2\pi c/9) - b\,q\sin(c\,\phi_2)\sin(2\pi c/9) \quad (A9)$$

Subtract (A8) from (A4)

$$p_2 - p_1 = b\,q\left[\cos(c\,\phi_2)\left[1 - \cos(2\pi c/9)\right] - \sin(c\,\phi_2)\sin(2\pi c/9)\right] \quad (A10)$$

Similarly

$$p_3 - p_2 = b\,q\left[\cos(c\,\phi_2)\left[\cos(2\pi c/9) - 1\right] - \sin(c\,\phi_2)\sin(2\pi c/9)\right] \quad (A11)$$

Square and add (A10) and (A11)

$$\begin{aligned}(p_2-p_1)^2 + (p_3-p_2)^2 &= 2\,b^2q^2\Big[\cos^2(c\,\phi_2)\left[1 - \cos(2\pi c/9)\right]^2 \\ &\quad + \sin^2(c\,\phi_2)\left[1 - \cos(2\pi c/9)\right]\left[1 - \cos(2\pi c/9)\right]\Big] \\ &= 2\,b^2q^2\left[1 - \cos(2\pi c/9)\right]\{1 - \cos(2\pi c/9) \\ &\quad + 2\cos(2\pi c/9)\sin^2(c\,\phi_2)\} \quad (A12)\end{aligned}$$

Combine (A8) and (A9)

$$p_3 - p_1 = -\,2\,b\,q\sin(c\,\phi_2)\sin(2\pi c/9)$$

Solve for $\sin(c\,\phi_2)$

$$\sin(c\,\phi_2) = -\frac{(p_3-p_2)+(p_2-p_1)}{2\,b\,q\,\sin(2\pi c/9)} \tag{A13}$$

Substitute (A13) in (A12)

$$(p_2-p_1)^2+(p_3-p_2)^2 = 2\,b^2q^2\left[1-\cos(2\pi c/9)\right]^2 + \frac{\left[(p_3-p_2)^2+2(p_3-p_2)(p_2-p_1)+(p_2-p_1)^2\right]\cos(2\pi c/9)}{1+\cos(2\pi c/9)}$$

Solve for q

$$q = \frac{1}{b\left[1-\cos(2\pi c/9)\right]}\left[\frac{(p_2-p_1)^2-2\cos(2\pi c/9)(p_2-p_1)(p_3-p_2)+(p_3-p_2)^2}{2\left[1+\cos(2\pi c/9)\right]}\right]^{\frac{1}{2}} \tag{A14}$$

In terms of the constants of (A1),

$$q = \frac{2}{A\left[1-\cos(4\pi B/9)\right]}\left[\frac{(p_2-p_1)^2-2\cos(4\pi B/9)(p_2-p_1)(p_3-p_2)+(p_3-p_2)^2}{2\left[1+\cos(4\pi B/9)\right]}\right]^{\frac{1}{2}} \tag{A15}$$

The flow direction with respect to the middle orifice is obtained by substituting (A14) into (A13)

$$\sin(c\,\phi_2) = -\left[\frac{1-\cos(2\pi c/9)}{2}\right]^{\frac{1}{2}} \frac{(p_3-p_2)+(p_2-p_1)}{\left[(p_2-p_1)^2-2\cos(2\pi c/9)(p_2-p_1)(p_3-p_2)+(p_3-p_2)^2\right]^{\frac{1}{2}}}$$

$$\phi_2 = \frac{-1}{2B}\sin^{-1}\left\{\frac{\left[\frac{1-\cos(4\pi B/9)}{2}\right]^{\frac{1}{2}}\left[(p_3-p_2)+(p_2-p_1)\right]}{\left[(p_2-p_1)^2-2\cos(4\pi B/9)(p_2-p_1)(p_3-p_2)+(p_3-p_2)^2\right]^{\frac{1}{2}}}\right\} \tag{A16}$$

The angle ϕ_2 is measured from the stagnation point to the middle orifice. The angle from the middle orifice to the stagnation point, measured in the direction of increasing orifice number, is

$$\phi = - \phi_2 \ . \qquad \text{(A17)}$$

REFERENCES

1. Fage, A. and Falkner, V. M.: Further Experiments on the Flow Around a Circular Cylinder. R. and M. No. 1369, British A. R. C., 1931.

2. Gowen, F. E. and Perkins, E. W.: Drag of Circular Cylinders for a Wide Range of Reynolds Numbers and Mach Numbers. NACA TN 2960, 1953.

3. Amick, J. L.: Pressure Measurements on Sharp and Blunt 5° and 15° Half-Angle Cones at Mach Number 3.86 and Angles of Attack to 100°. NASA TN D-753, 1961.

4. Bursnall, W. J. and Loftin, L. K. Jr.: Experimental Investigation of the Pressure Distribution About a Yawed Circular Cylinder in the Critical Reynolds Number Range. NACA TN 2463, 1951.

THE UNIVERSITY OF MICHIGAN

DATE DUE

4/11 16:33